

TIPP 2011 - Technology and Instrumentation for Particle Physics 2011

Crystal calorimeters in the next decade

Ren-yuan Zhu¹

256-48, HEP, California Institute of Technology, Pasadena, CA 91125, USA

Abstract

Crystal calorimeter has traditionally played an important role in precision measurement of electrons and photons in high energy physics experiments. Recent interest in calorimeter technology extends its application to measurement of hadrons and jets with dual readout. Potential application of new generation scintillating crystals of high density and high light yield, such as cerium doped LSO and LYSO, in high energy physics experiments is described. Candidate crystals for the homogeneous hadronic calorimeter concept are also discussed.

© 2012 Published by Elsevier B.V. Selection and/or peer review under responsibility of the organizing committee for TIPP 11.

Keywords: Crystal; Scintillator; Calorimeter; Dual Readout; Homogeneous Hadronic Calorimeter.

1. Introduction

Total absorption shower counters made of inorganic crystal scintillators have been known for decades for their superb energy resolution and detection efficiency for electrons and photons [1]. In high energy and nuclear physics, crystal calorimeters have been constructed, and their use has been a key factor in the successful physics programs of many experiments. The physics discovery potential of crystal calorimeter was early demonstrated by the Crystal Ball experiment through its study of radiative transitions and decays of the Charmonium family [2]. With proper calibration and monitoring, crystal calorimeters usually achieve their designed resolution *in situ* [3].

Table 1 summarizes parameters of past and present crystal electromagnetic calorimeters in high energy physics. One notes that each of these calorimeters requires several cubic meters of high quality crystals. The most ambitious crystal calorimeter is presumably the CMS calorimeter which uses 11 m³ PbWO₄ crystals. Its designed energy resolution [4] is

$$\sigma_E/E = 2.7\%/\sqrt{E} \oplus 0.55\% \oplus 0.16/E \quad (1)$$

for the barrel, and

$$\sigma_E/E = 5.7\%/\sqrt{E} \oplus 0.55\% \oplus 0.77/E \quad (2)$$

for the endcaps.

¹Corresponding author. Tel.: +1-626-395-6661; fax: +1-626-795-3951; E-mail address: zhu@hep.caltech.edu.

Table 1. Crystal Calorimeter in High Energy Physics: Past and Present

Experiment	C. Ball	L3	CLEO II	KTeV	<i>BaBar</i>	BELLE	CMS
Accelerator	SPEAR	LEP	CESR	Tevatron	PEP II	KEK	LHC
Date	75–85	80–00	80–00	90–10	94–10	94–10	95–20
Crystal Type	NaI(Tl)	BGO	CsI(Tl)	CsI	CsI(Tl)	CsI(Tl)	PbWO ₄
B-Field (Tesla)	-	0.5	1.5	-	1.5	1.0	4.0
Inner Radius (m)	0.254	0.55	1.0	-	1.0	1.25	1.29
Number of Crystals	672	11,400	7,800	3,300	6,580	8,800	76,000
Crystal Depth (X_0)	16	22	16	27	16 to 17.5	16.2	25
Crystal Volume (m ³)	1	1.5	7	2	5.9	9.5	11
L. Yield (p.e./MeV)	350	1,400	5,000	40	5,000	5,000	2
Photo-sensor	PMT	Si PD	Si PD	PMT	Si PD	Si PD	APD [†]
Photo-sensor Gain	Large	1	1	4,000	1	1	50
Noise/Can. (MeV)	0.05	0.8	0.5	Small	0.15	0.2	30
Dynamic Range	10 ⁴	10 ⁵	10 ⁴	10 ⁴	10 ⁴	10 ⁴	10 ⁵

† Avalanche photo-diode.

This energy resolution can be decomposed to three contributions from photo-electron statistics (stochastic), intrinsic shower leakage (stochastic and constant) and readout noise (noise). Result of electron beam tests at CERN shows a good agreement with Equation 1 for two groups of 3×3 crystals, independent of their impact position on the crystal front face [5]. Recent interest in homogeneous hadronic calorimeter (HHCAL) extends crystal's application to measurement of hadrons and jets with high resolution [6]. This HHCAL detector concept adapts dual readout for both Cherenkov and scintillation light, which is extensively studied recently by the Dream collaboration [7].

Section 2 of this paper describes optical and scintillation properties of heavy crystal scintillators commonly used in particle physics experiment. Fast and bright crystals discovered in the last two decades, such as cerium doped lutetium oxyorthosilicate ($\text{Lu}_2(\text{SiO}_4)\text{O}$ or LSO) [8], cerium doped lutetium yttrium oxyorthosilicate ($\text{Lu}_{2(1-x)}\text{Y}_{2x}\text{SiO}_5$, LYSO) [9] and cerium doped lanthanum tri-halides, e.g. LaCl_3 and LaBr_3 [10] are also covered. The expected performance of an LSO/LYSO electromagnetic calorimeter is elaborated in Section 3. Section 4 discusses candidate crystals for the HHCAL detector concept.

2. Properties of Crystal Scintillators

Table 2 lists basic properties of heavy crystals with mass production capability: NaI(Tl), CsI(Tl), BaF_2 , CeF_3 , bismuth germanate ($\text{Bi}_4\text{Ge}_3\text{O}_{12}$ or BGO), lead tungstate (PbWO_4 or PWO), LSO/LYSO [11] and PbF_2 . All, except PbF_2 , are scintillators with the characteristics of their scintillation light listed. All, except CeF_3 , have either been used in, or actively pursued for, high energy and nuclear physics experiments, which are also listed in the table. The experiment name in bold indicates the future crystal calorimeters in the next decade. LSO and LYSO crystals are also widely used in the medical industry. Mass production capabilities exist for all these crystals.

Figure 1 is a photo showing twelve crystal scintillator samples. In addition to samples listed in Table 2 pure CsI, CsI(Na), LYSO as well as LaCl_3 and LaBr_3 are also shown in this photo although the last two are not yet in mass production stage. Samples are arranged in an order of their density, or radiation length. All non-hygroscopic samples are wrapped with white Tyvek paper as reflector. Hygroscopic NaI, CsI, LaBr_3 and LaCl_3 are sealed in package with two ends made of quartz windows of 3 or 5 mm thick to avoid surface degradation. To minimize uncertainties in light output measurement caused by the sample size dependence all samples have a cubic shape of $1.5 \times 1.5 \times 1.5 X_0^3$, except NaI(Tl) and LaCl_3 which are a cylinder with a length of $1.5 X_0$ and areas at two ends equaling to $1.5 \times 1.5 X_0^2$ to match the 2 inch diameter of the PMT cathode.

Table 2. Properties of Heavy Crystal with Mass Production Capability

Crystal	NaI(Tl)	CsI(Tl)	BaF ₂	CeF ₃	BGO	PbWO ₄	LSO(Ce)	PbF ₂
Density (g/cm ³)	3.67	4.51	4.89	6.16	7.13	8.3	7.40	7.77
Melting Point (°C)	651	621	1280	1460	1050	1123	2050	824
Radiation Length (cm)	2.59	1.86	2.03	1.70	1.12	0.89	1.14	0.93
Molière Radius (cm)	4.13	3.57	3.10	2.41	2.23	2.00	2.07	2.21
Interaction Length (cm)	42.9	39.3	30.7	23.2	22.7	20.7	20.9	21.0
Refractive Index ^a	1.85	1.79	1.50	1.62	2.15	2.20	1.82	1.82
Hygroscopicity	Yes	Slight	No	No	No	No	No	No
Luminescence ^b (nm)	410	560	300 220	340 300	480	425 420	420	?
Decay Time ^b (ns)	245	1220	650 0.9	30	300	30 10	40	?
Light Yield ^{b,c}	100	165	36 4.1	7.3	21	0.30 0.077	85	?
d(LY)/dT ^{b,d} (%/°C)	-0.2	0.4	-1.9 0.1	~0	-0.9	-2.5	-0.2	?
Experiment	Crystal Ball	CLEO <i>BaBar</i> BELLE BES III	TAPS	-	L3 BELLE	CMS ALICE PrimEx Panda	Mu2e SuperB SLHC?	A4 HHCAL?

a At the wavelength of the emission maximum.

b Top line: slow component, bottom line: fast component.

c Relative light yield of samples of 1.5 X₀ and with the PMT quantum efficiency taken out.

d At room temperature.

Figure 2 shows a comparison of the transmittance, emission and excitation spectra for ten samples. The solid black dots in these plots are the theoretical limit of the transmittance, which is calculated by using corresponding refractive index as a function of wavelength taking into account multiple bounces between the two parallel end surfaces and assuming no internal absorption [12]. Most samples, except LaBr₃ and

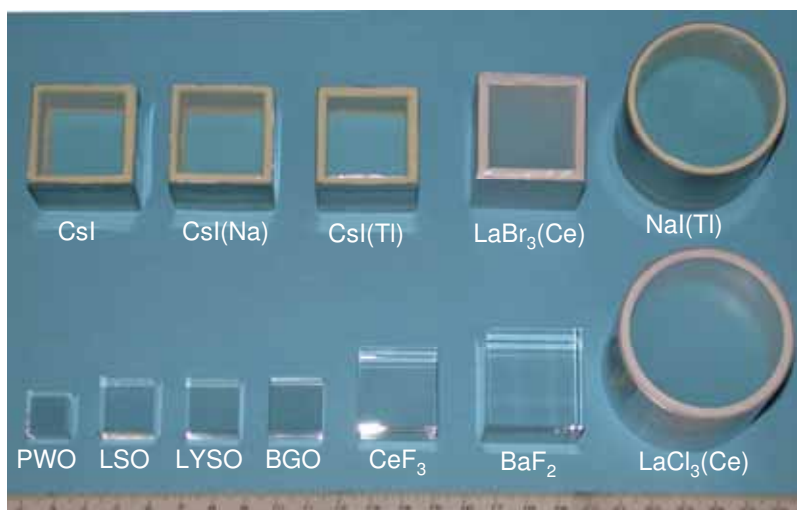


Fig. 1. A photo shows twelve crystal scintillators with dimension of 1.5 X₀.

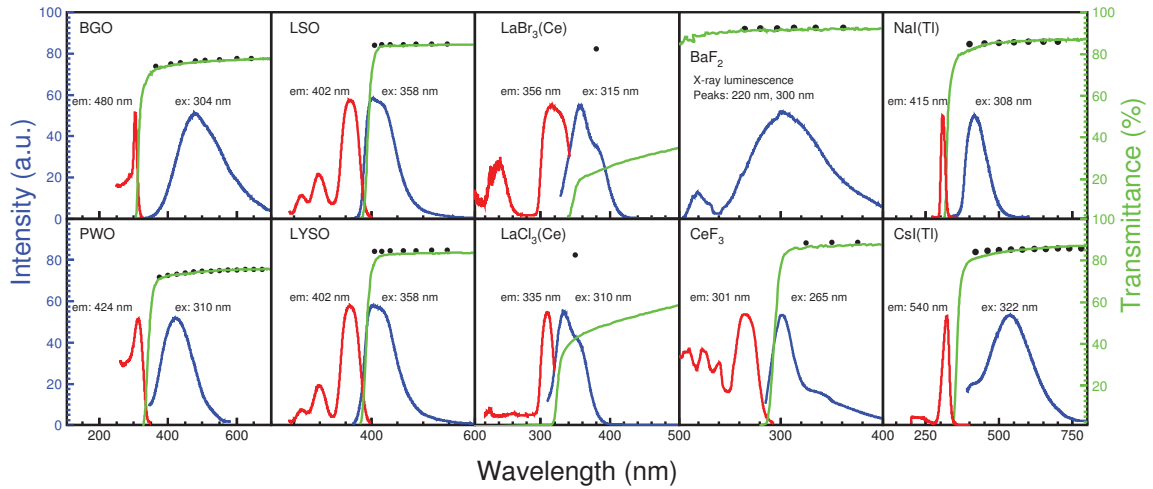


Fig. 2. The excitation (red) and emission (blue) spectra (left scale) and the transmittance (green) spectra (right scale) are shown as a function of wavelength for ten crystal scintillators. The solid black dots are the theoretical limit of the transmittance.

LaCl₃, have their transmittance approaching the theoretical limits, indicating negligible internal absorption. The poor transmittance measured for LaBr₃ and LaCl₃ samples is probably due to scattering centers inside these samples. It is interesting to note that BaF₂, BGO, NaI(Tl), CsI(Tl) and PbWO₄ have their emission spectra well within the transparent region showing no obvious self-absorption effect. The UV absorption edge in the transmittance spectra of LSO, LYSO, CeF₃, LaBr₃ and LaCl₃, however, cuts into the emission spectra and thus affects crystal's light output. This self-absorption effect is more seriously in long crystal samples used in high energy and nuclear physics experiment as extensively discussed for LSO and LYSO crystals [13]. We also note that the values of the cut-off wavelength, at which the transmittance data show 50% of that at 800 nm, are 140 nm, 280 nm, 293 nm, 315 nm, 318 nm, 342 nm, 358 nm, 365 nm and 390 nm for BaF₂, CsI, CeF₃, BGO, CsI(Na), PWO, CsI(Tl), NaI(Tl) and LSO/LYSO respectively, while it is 250 nm for PbF₂.

Figure 3 shows the ¹³⁷Cs γ -ray pulse high spectra measured by a Hamamatsu R1306 PMT with bi-alkali cathode for twelve crystal samples. Also shown in these figures are the corresponding FWHM energy resolution (E.R.). γ -ray spectroscopy with a few percents resolution is required to identify isotopes for the homeland security applications. It is clear that only LaBr₃ approaches this requirement. All other crystals do not provide sufficient energy resolution at low energies.

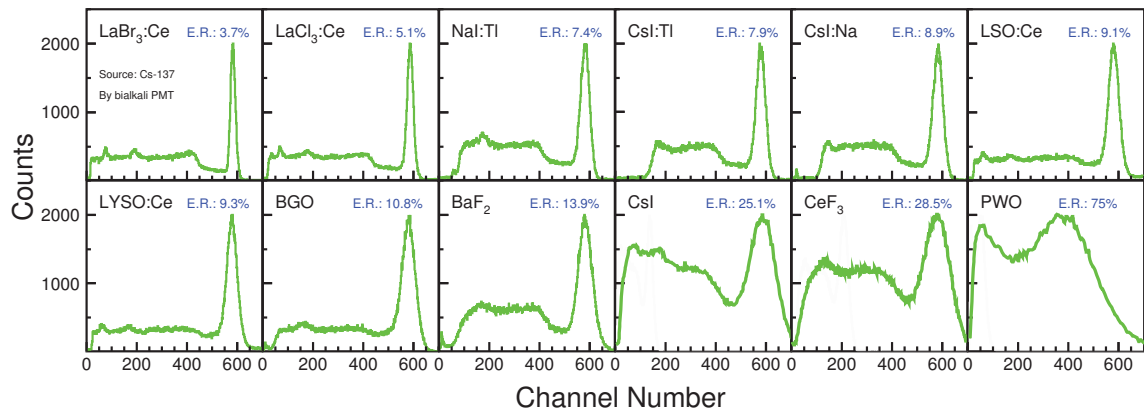


Fig. 3. ¹³⁷Cs γ -ray pulse high spectra measured by a Hamamatsu R1306 PMT are shown for twelve crystal samples. The numerical values of the FWHM resolution (E.R.) are also shown in the figure.

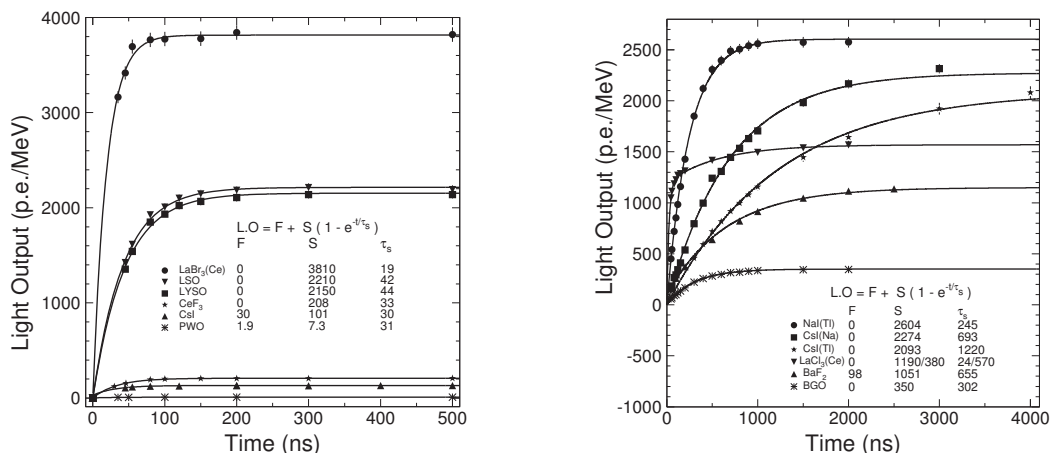


Fig. 4. Light output measured by using a XP2254b PMT is shown as a function of integration time for six fast (Left) and six slow (Right) crystal scintillators.

Figure 4 shows light output in photo-electrons per MeV energy deposition as a function of the integration time, measured by using a Photonis XP2254b PMT with multi-alkali photo cathode, for six fast crystal scintillators (Left): LaBr₃, LSO, LYSO, CeF₃, un-doped CsI and PbWO₄ and six slow crystal scintillators (Right): NaI(Tl), CsI(Na), CsI(Tl), LaCl₃, BaF₂ and BGO. The corresponding fits to the exponentials and their numerical results are also shown in these figures. The un-doped CsI, PbWO₄, LaCl₃ and BaF₂ crystals are observed to have two decay components. Despite its poor transmittance the cerium doped LaBr₃ is noticed by its bright fast scintillation, leading to the excellent energy resolution for the γ -ray spectroscopic applications. The LSO and LYSO samples have consistent fast decay time (~ 40 ns) and photo-electron yield, which is 6 and 230 times of BGO and PbWO₄ respectively.

Since the quantum efficiency of the PMT used for the light output measurement is a function of wavelength, it should be taken out to directly compare crystal's light output. Figure 5 shows typical quantum efficiency as a function of wavelength for a PMT with bi-alkali cathode (Hamamatsu R1306) and a PMT with multi-alkali cathode (Photonis 2254B), a Si APD (Hamamatsu S8664) and a Si PIN PD (Hamamatsu

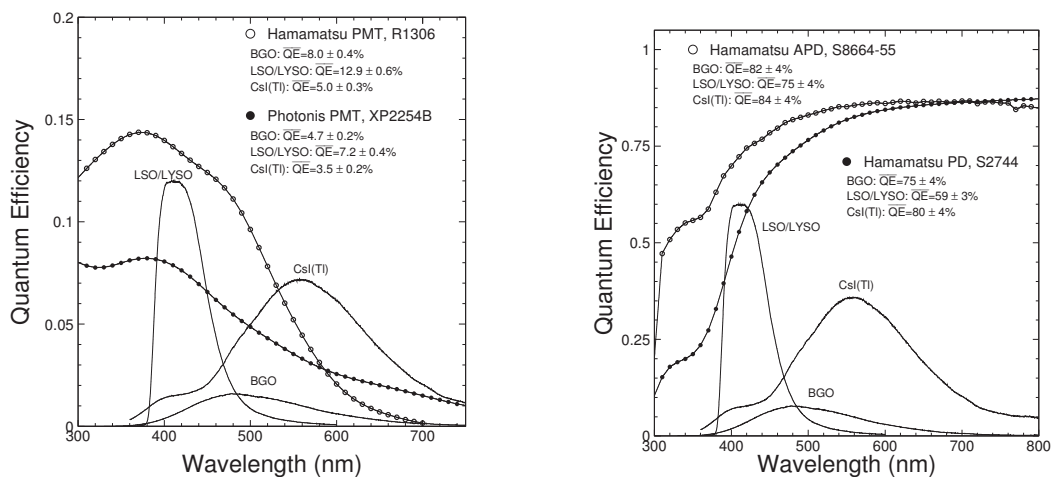


Fig. 5. Left: Quantum efficiencies of a Hamamatsu 1306 PMT with bi-alkali cathode (open circles) and a Photonis 2254B PMT with multi-alkali cathode (solid dots) are shown as a function of wavelength together with the emission spectra of the LSO/LYSO, BGO and CsI(Tl) samples, where the area under the emission curves is proportional to their corresponding absolute light output. Right: The same for a Hamamatsu S8664 Si APD (open circles) and a Hamamatsu S2744 Si PIN diode (solid dots).

S2744). The emission spectra of LSO/LYSO, BGO and CsI(Tl) crystals are also shown in these figures. The light output values in Table 2 are listed with the PMT quantum efficiency taken out. The light output of LSO and LYSO crystals is a factor of 4 and 200 of that of BGO and PbWO_4 respectively.

Scintillation light yield of crystals may also depend on the temperature. Fig 6 shows light output variations for twelve crystal samples between 15°C and 25°C . The corresponding temperature coefficients obtained from linear fits are also listed in the figure. The numerical result of these fits is also listed in Table 2.

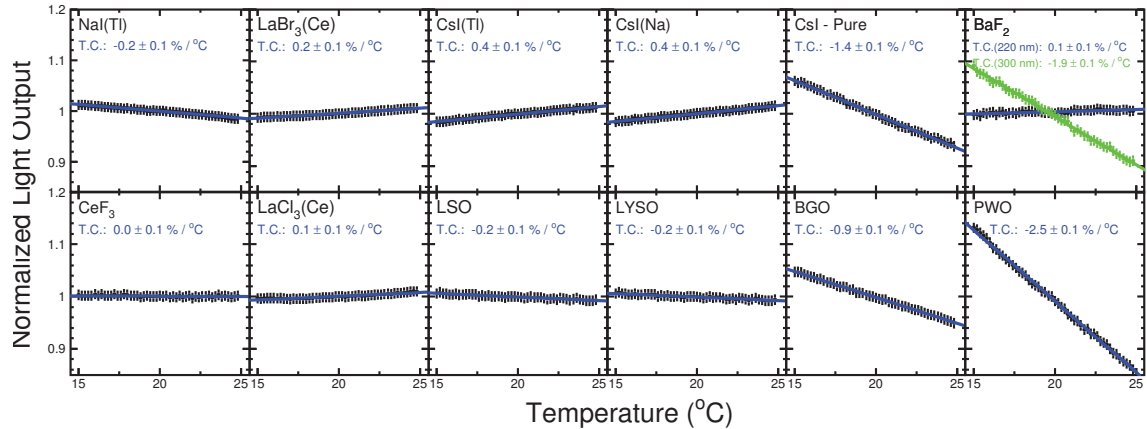


Fig. 6. Light output temperature coefficient obtained from linear fits between 15°C and 25°C for twelve crystal scintillators.

3. LSO/LYSO Crystal Electromagnetic Calorimeter

Because of their broad application in medical industry large size LSO and LYSO crystals with consistent optical and scintillation properties have been routinely grown [13]. Figure 7 shows four long crystal samples of $2.5 \times 2.5 \times 20 \text{ cm}^3$. Figure 8 shows the spectra of 0.51 MeV γ -rays from a ^{22}Na source observed with coincidence triggers [13]. The readout devices used are a Hamamatsu R1306 PMT (Left) and 2 Hamamatsu

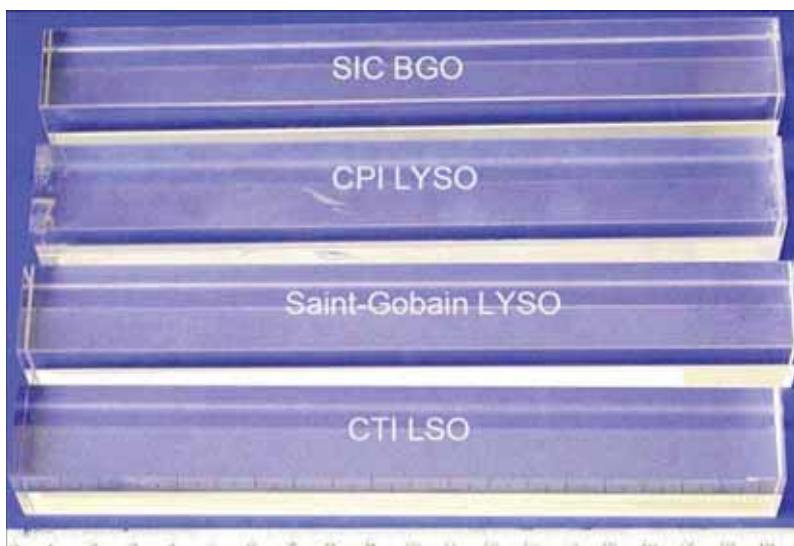


Fig. 7. A photo shows four long crystal samples with dimension of $2.5 \times 2.5 \times 20 \text{ cm}^3$.

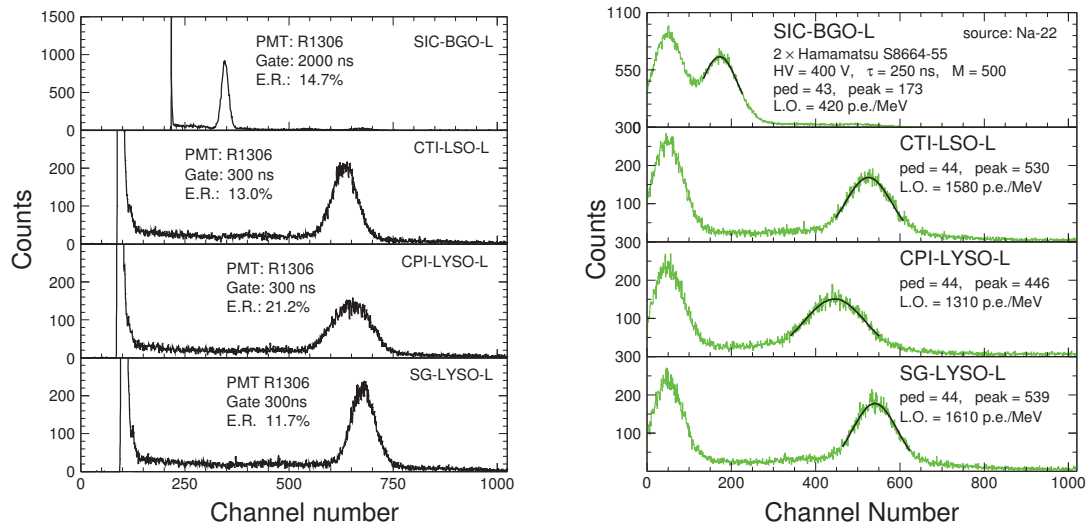


Fig. 8. The 0.511 MeV γ -rays spectra from a ^{22}Na source measured with a coincidence trigger using a Hamamatsu R1306 PMT (Left) and two Hamamatsu S8664-55 APDs (Right) for long BGO, LSO and LYSO samples of $2.5 \times 2.5 \times 20 \text{ cm}^3$ size.

S8664-55 APDs (Right). The FWHM resolution for the 0.51 MeV γ -ray with the PMT readout is about 12% to 13% for these long samples, which can be compared to 15% for the BGO sample. With APD readout, the γ -ray peaks are clearly visible. The energy equivalent readout noise was less than 40 keV for these long LSO and LYSO samples.

LSO/LYSO crystals is also found to be much more radiation hard than other crystals commonly used in high energy and nuclear physics experiment, such as BGO, CsI(Tl) and PbWO_4 [14]. Their scintillation mechanism is not damaged by γ -ray irradiation. Radiation damage in LSO and LYSO crystals recovers very slow under room temperature but can be completely cured by thermal annealing at 300°C for ten hours. The γ -ray induced readout noise was estimated to be about 0.2 MeV and 1 MeV equivalent respectively in a

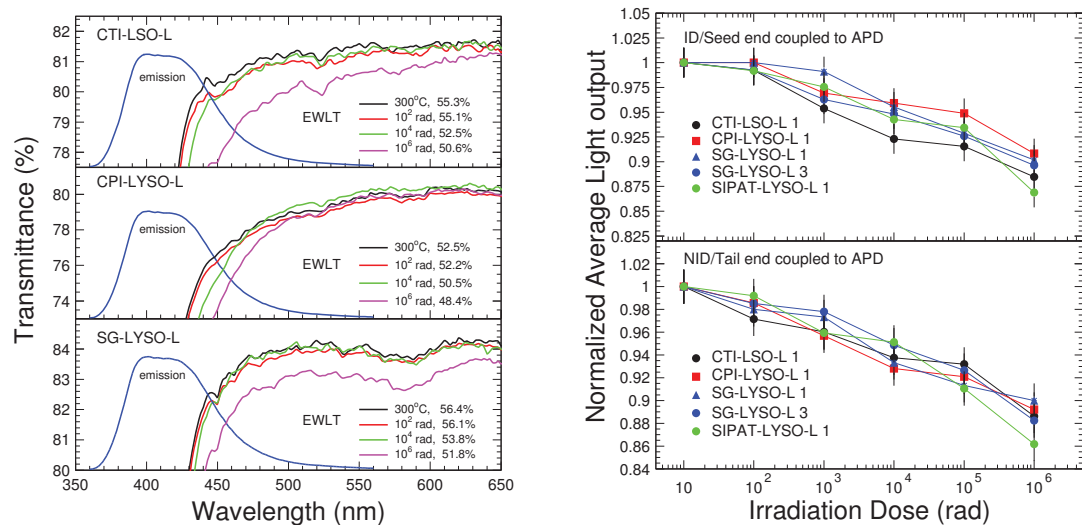


Fig. 9. Left: Transmittance spectra are shown as a function of wavelength in an expanded scale together with the photo-luminescence spectra for three long LSO and LYSO samples before and after the irradiation with integrated doses of 10^2 , 10^4 and 10^6 rad. Right: Normalized light output with ID (top) and NID (bottom) end coupled to the readout device of two S8664-55 APDs is shown as a function of the integration dose for five long LSO and LYSO samples.

radiation environment of 15 rad/h and 500 rad/h for LSO and LYSO samples of $2.5 \times 2.5 \times 20 \text{ cm}^3$.

Figure 9 (Left) shows an expanded view of the longitudinal transmittance spectra for three samples before and after several steps of the γ -ray irradiation with integrated dose of 10^2 , 10^4 and 10^6 rad. Also shown in the figure is the corresponding numerical values of the photo-luminescence weighted longitudinal transmittance (*EWLT*). Figure 9 (Right) shows the normalized average light output as a function of integrated dose for five long samples from various vendors. It is interesting to note that all samples show consistent radiation resistance with degradations of both the light output and transmittance at 10 to 15% level after γ -ray irradiation with an integrated dose of 1 Mrad.

Assuming the same APD based readout scheme as the CMS PbWO_4 calorimeter, the expected energy resolution of an LSO/LYSO crystal based electromagnetic calorimeter would be

$$\sigma_E/E = 2\%/\sqrt{E} \oplus 0.5\% \oplus 0.001/E, \quad (3)$$

which represents a fast calorimeter over large dynamic range with low noise. Such calorimeter would provide great physics discovery potential for high energy physics experiments in the proposed SuperB factory [15] as well as the proposed International Linear Collider (ILC) [16]. Because of its fast scintillation and good radiation hardness LYSO crystals are also proposed for the CMS PbWO_4 crystal endcap calorimeter upgrade at SLHC [17].

4. Homogeneous Hadronic Calorimeter Detector Concept

Crystals have recently been proposed to construct a homogeneous calorimeter, including both electromagnetic and hadronic part [6]. This HHCAL detector concept removes the traditional boundary between ECAL and HCAL, so eliminates the effect of dead materials in the middle of the hadronic shower development. It takes advantage of recently implemented dual readout approach to measure both Cherenkov and scintillation light to achieve good energy resolution for hadronic jets measurement [7]. Because of the un-precedent volume (70 to 100 m^3) foreseen for such calorimeter [6], the crystal material must be dense (to reduce the volume), UV transparent (to effectively collecting the Cherenkov light) and allows a clear discrimination between the Cherenkov and scintillation light.

Figure 10 (Left) shows samples of three $5 \times 5 \times 5 \text{ cm}^3$ crystal samples: PbF_2 , BGO and PWO. Crystals of this size can be seen as typical building block for a crystal hadronic calorimeter. All material are dense (PbF_2 has a density of 7.7 g/cm^3) with a nuclear interaction length about 22 cm. Figure 10 (Right) shows the transmittance spectra of PbF_2 (green), BGO (blue), PWO (red) and a UG11 filter (black) as a function of wavelength together with the Cherenkov emission spectrum (dashed blue). The UG 11 filter can be used to select the Cherenkov light with small or no scintillation contamination. Also shown in this

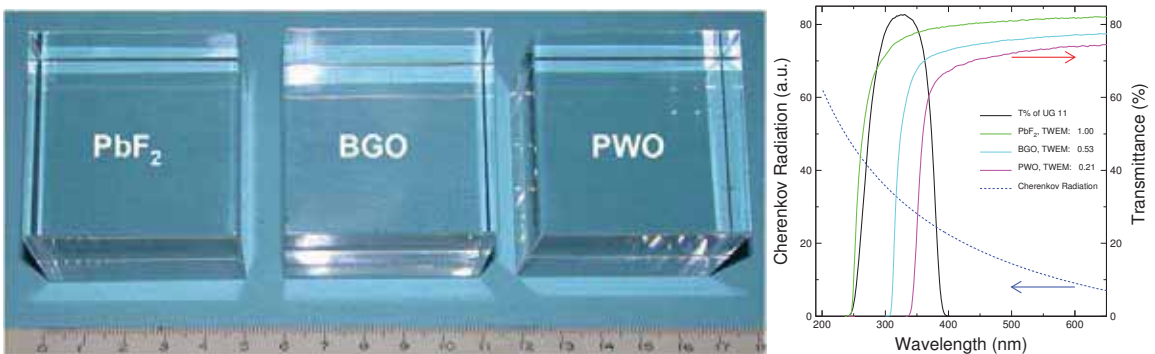


Fig. 10. Left: A photo shows three crystal samples of $5 \times 5 \times 5 \text{ cm}^3$ investigated for the homogeneous hadronic calorimeter concept. Right: The transmittance spectra of PbF_2 (green), BGO (blue), PWO (red) and UG11 (black) are shown as a function of wavelength. Also shown in this figure are the Cherenkov emission spectrum (dashed blue) and the normalized figure of merit for the Cherenkov light measurement with the UG11 filter.

figure is the normalized figure of merit for the Cherenkov measurement (TWEM) by using the UG11 filter, which is defined as the transmittance weighted Cherenkov emission spectrum. Their numerical values are 1.0:0.53:0.21, which would be 1.0:0.82:0.75 without using the UG11 filter. Among these materials PbF_2 is the most effect in collecting the Cherenkov light because of its good UV transmission.

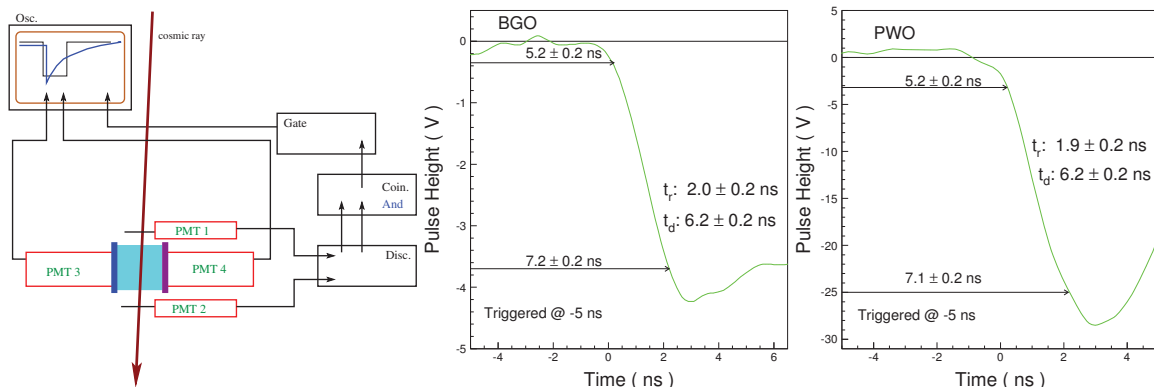


Fig. 11. Left: A schematic showing a simple set-up used to measure cosmic-ray generated Cherenkov and scintillation light simultaneously by using two Hamamatsu R2059 PMT. The light pulses are recorded by an Agilent 6052A digital scope. Digital scope traces of the scintillation light front edge measured by a Hamamatsu R2059 PMT with GG400 filter for the BGO (Middle) and PWO (Right) samples.

Effective discrimination between Cherenkov and scintillation light can be realized by using optical filter. Figure 11 (Left) shows a set-up used to investigate Cherenkov light collection and its separation from the scintillation light. Cosmic-rays were triggered by two finger counters with coincidence. The Cherenkov and scintillation light pulses generated by cosmic-rays were measured simultaneously by two Hamamatsu R2059 PMT coupled to the sample through optical filters UG11 and GG400. GG400 is a low-pass filter with cut-off at 400 nm. The UG11 filter is used to select the Cherenkov light as shown in Figure 10 (Right). The GG400 filter is used to select the scintillation light with small contamination of the Cherenkov light. The output of these two PMTs were digitized by an Agilent 6052A digital scope. Figure 11 (Middle and Right) shows the front edge of the scintillation light pulse from BGO and PWO, observed through the GG400 filter. Their delay from the trigger (t_d) and rise time (t_r) are identical with numerical values of 6.2 ns and 1.9 ns respectively. Figure 12 shows the Cherenkov light pulse shape observed for PbF_2 (Left), BGO (Middle) and PWO (Right) through the UG11 filter. All pulses have consistent time structure in the delay (6.1 ns), the rise time (1.8 ns), the fall time (4.2 ns) and the FWHM width (3.0 ns). It is interesting to note that there is

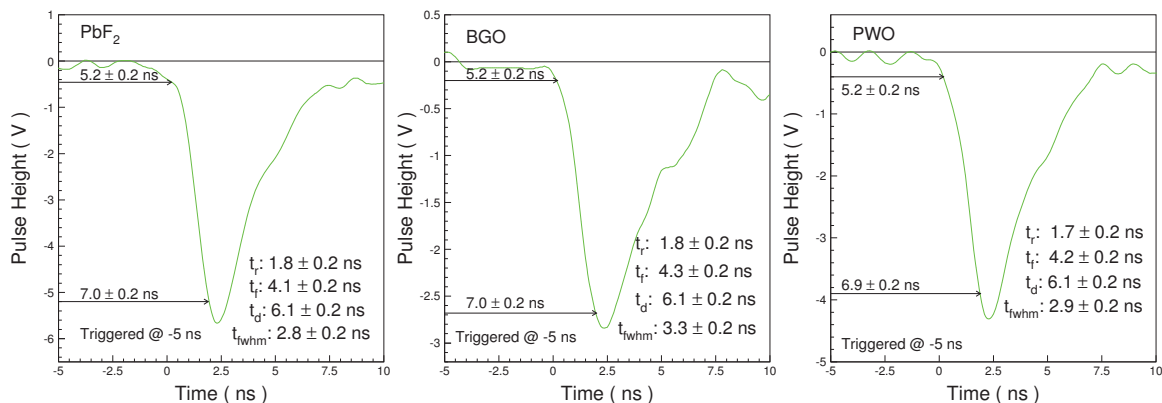


Fig. 12. Digital scope traces of Cherenkov light pulse measured by a Hamamatsu R2059 PMT with UG11 filter for the PbF_2 (Left), BGO (Middle) and PWO (Right) samples.

no difference observed in the delay and rise time between the Cherenkov and scintillation light, indicating that only the light pulse width and fall time are useful for the discrimination between the Cherenkov and scintillation light. A slow scintillator may actually help this discrimination. The ratio of Cherenkov versus scintillation light was measured to be 1.55% and 22% for BGO and PWO respectively. These values are consistent with the scintillation light yield shown in Table 2, the emission weighed quantum efficiency of bi-alkali cathode of the Hamamatsu R2059 PMT shown in Figure 5 (Left) and the TWEM values shown in Figure 10 (Right).

Based upon our experience accumulated in building crystal ECAL, an initial detector design with pointing geometry was proposed. It may provide a better resolutions for both energy and position measurements, and thus a good jet mass reconstruction. Figure 13 shows a schematic of a typical HHCAL cell with pointing geometry [18]. It is similar to a typical calorimeter cell of a crystal ECAL, but has several longitudinal segments with a total length of about 1 m. By using dense active materials such detector depth would provide about 5 nuclear interaction lengths, adequate for the hadronic jet energy reconstruction. The readout devices are mounted on the side faces of these crystal segments. Due to the recent development in compact solid state readout devices, e.g. silicon PMT, such a readout scheme is now feasible.

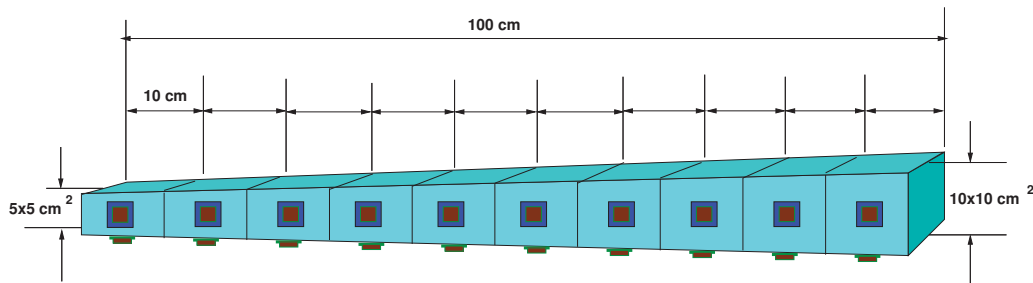


Fig. 13. A schematic showing a typical cell for the HHCAL detector concept with pointing geometry [18].

Because of the huge volume required for the HHCAL detector concept development of cost-effective material is crucial. Table 3 summarized the basic property of candidate crystals being considered for this detector concept. While BGO is the best material to be used for such calorimeter its mass production cost is prohibitive. While PWO, PbF₂, PbFCl and BSO are under investigation, PbF₂ and PbFCl are preferred because of its low melting point and raw material cost.

Table 3. Candidate Crystals for the HHCAL Detector Concept

Parameters	BGO	PWO	PbF ₂	PbFCl	BSO
Density (g/cm ³)	7.13	8.29	7.77	7.11	6.8
λ_I (cm)	22.8	20.7	21.0	24.3	23.1
$n @ \lambda_{max}$	2.15	2.20	1.82	2.15	2.06
τ_{decay} (ns)	300	30/10	?	30	100
λ_{max} (nm)	480	425/420	?	420	470
Cut-Off λ (nm)	310	350	250	280	300
Light Output (%)	100	1.4/0.37	?	17	20
Melting Point (°C)	1050	1123	842	608	1030
Raw Material Cost (%)	100	49	29	29	47

R&D is actively pursued by the high energy physics community for additional materials. One approach is to develop PWO crystals with slow scintillation emission. Green (560 nm) and slow emission with a few μ sec decay time was observed by selective doping in PWO crystals [19]. Such crystals were reported to have a factor of ten more light than yttrium doped PWO crystals used in high energy physics experiment.

This slow and green scintillation would be desirable for this application.

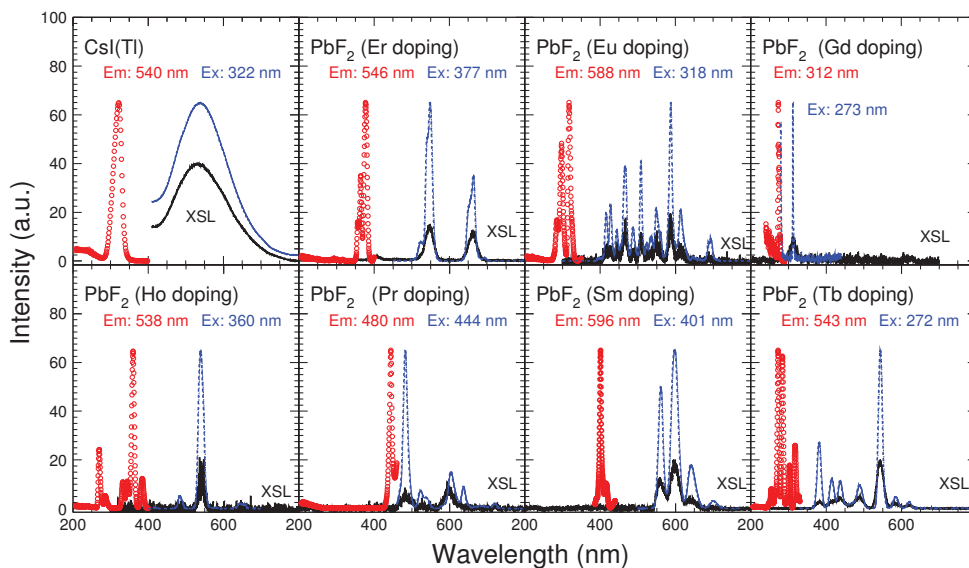


Fig. 14. The excitation (red dots) and Photo- (blue dashes) and X- (black lines) luminescence spectra are shown as a function of wavelength for the PbF₂ samples doped with Er, Eu, Gd, Ho, Pr, Sm and Tb as well as a reference CsI(Tl) sample.

Another approach is to develop scintillating PbF₂ crystals by selective doping. Observations of fast scintillation in Gd doped PbF₂ crystals were reported early by Shen and Woody [20, 21]. Our investigation shows that rear earth doping introduces scintillation in PbF₂, but not in the level can be measured by using γ -ray source [22]. Figure 14 show the excitation, photo-luminescence and x-luminescence spectra for Er, Eu, Gd, Ho, Pr, Sm and Tb doped PbF₂ crystal samples. It is noted that some of these scintillation lights is between 500 to 600 nm, which is desirable for Cherenkov/scintillation discrimination. Investigation is continuing aiming at developing cost-effective materials for this concept.

The photo-luminescence decay time constant of these doped PbF₂ samples was measured by using a

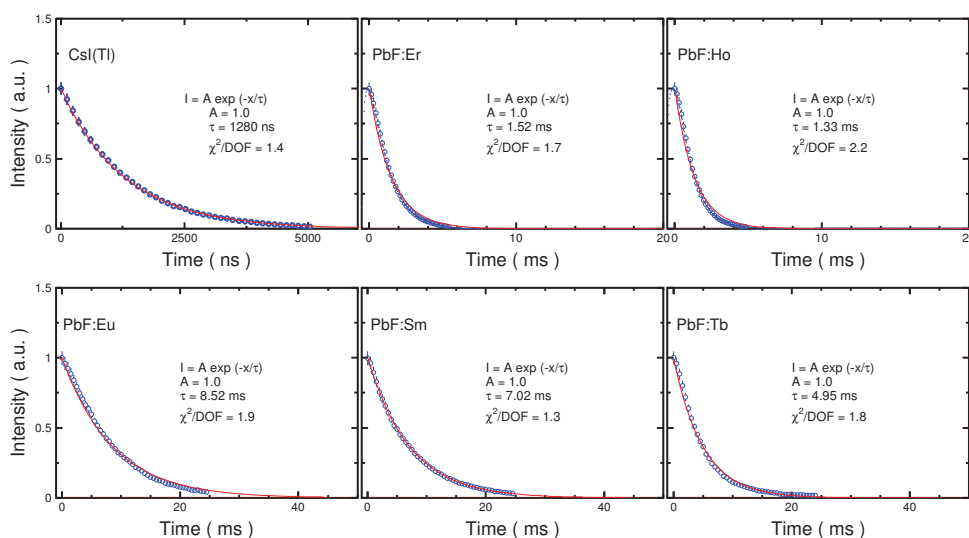


Fig. 15. The photo-luminescence pulse shape (blue circles), corresponding fit to an exponential (red lines) and the decay time constant are shown for the PbF₂ samples doped with Er, Ho, Eu, Sm and Tb as well as a reference CsI(Tl) sample.

pulsed laser as the excitation source. Figure 15 shows the photo-luminescence pulse shape (blue circles), the corresponding exponential fit (red lines) and the decay time constant for the PbF₂ samples doped with Er, Ho, Eu, Sm and Tb as well as a reference CsI(Tl) sample. The photoluminescence intensity of PbF₂ samples doped with Pr and Gd are too weak to be useful to extract the decay time constant. The decay time constants for the PbF₂ samples doped with Er, Ho, Eu, Sm and Tb were found at a millisecond scale as expected from the f-f transition of these rare earth elements [23]. These time constants are too long to be useful for high energy physics experiments. The work will concentrate on selective rare earth doping, other PbF₂ phases and mixtures [22].

5. Summary

Precision crystal electromagnetic calorimeters have been an important part of high energy physics detector. The availability of mass production capability of large size LSO and LYSO crystals provides an opportunity to build a LSO/LYSO crystal electromagnetic calorimeter with good energy resolution over a large dynamic range down to MeV level. Such calorimeter, if built, would greatly enhance the physics discovery potential for high energy and nuclear physics experiments in the next decade.

Recent interest in high energy physics community to pursue homogeneous hadronic calorimeter with dual readout opens a new area of crystal calorimetry to achieve good energy resolution for hadronic jets in the next decade. The main challenge for this concept is to develop cost effective heavy scintillators with good UV transmission and excellent Cherenkov/scintillation discrimination. Dense crystals, scintillating glasses and ceramics offer a very attractive implementation for this detector concept.

Acknowledgments

This work is partially supported by the U.S. Department of Energy Grant No. DE-FG03-92-ER40701 and the U.S. National Science Foundation Award PHY-0612805 and PHY-0516857.

References

- [1] G. Gratta, H. Newman and R.-Y. Zhu, *Annu. Rev. Nucl. Part. Sci.* **44** 453 (1994).
- [2] E. Bloom and C. Peck, *Ann. Rev. Nucl. Part. Sci.* **33** (1983) 143-197.
- [3] R.-Y. Zhu, *Nucl. Instr. and Meth.* **A537** (2005) 344.
- [4] *The CMS Electromagnetic Calorimeter Project*, CERN/LHCC 97-33 (1997).
- [5] P. Adzic *et al.*, *JINST* **2** P04004 (2007).
- [6] A. Para, FERMILAB-CONF-11-519-CD, and H. Wenzel *et al.*, FERMILAB-PUB-11-531-CD-E.
- [7] N. Akchurin *et al.*, *Nucl. Instr. and Meth.* **A537** (2005) 537.
- [8] C. Melcher, V.S. Patent 4958080 (1990) and 5025151 (1991).
- [9] D.W. Cooke, K.J. McClellan, B.L. Bennett, J.M. Roper, M.T. Whittaker and R.E. Muenchausen, *J. Appl. Phys.* **88** (2000) 7360 and T. Kimble, M Chou and B.H.T. Chai, *2002 IEEE NSS Conference Record*.
- [10] E. Loef, P. Dorenbos, E. Eijk, K. Kraemer and H. Guedel, *Nucl. Instr. and Meth.* **A486** (2002) 254.
- [11] R.H. Mao, L.Y. Zhang and R.-Y. Zhu, *IEEE Trans. Nucl. Sci.* **NS-55** (2008).
- [12] D.A. Ma and R.-Y. Zhu, *Nucl. Instr. and Meth.* **A333** (1993) 422.
- [13] J.M. Chen, R.H. Mao, L.Y. Zhang and R.-Y. Zhu, *IEEE Trans. Nucl. Sci.* **54** (2007) 718.
- [14] J.M. Chen, R.H. Mao, L.Y. Zhang and R.-Y. Zhu, *IEEE Trans. Nucl. Sci.* **54** (2007) 1319.
- [15] SuperB Conceptual Design Report, **INFN/AE-07/2, SLAC-R-856, LAL 07-15**, March (2007).
- [16] R.-Y. Zhu, talk presented in 2005 ILC Workshop, Snowmass. <http://nicadd.niu.edu/cdsagenda/fullAgenda.php?ida=a0561>.
- [17] R.-Y. Zhu, talk presented in SCINT 2011 Conference, Giessen. http://www.hep.caltech.edu/~zhu/talks/ryz_I110913_scint_lyso.pdf.
- [18] R.-Y. Zhu, talk presented in International Linear Collider Workshop 2008 at Chicago. http://www.hep.caltech.edu/~zhu/talks/ryz_081118_lcws.pdf.
- [19] R.H. Mao *et al.*, in *Proceedings of IX International Conference on Calorimetry in Particle Physics*, Ed. B. Aubert *et al.*, Frascati Physics Series Vol. XXI (2000) 709-720.
- [20] D. Shen *et al.*, *Jour. Inor. Mater.* **Vol 101** (1995) 11.
- [21] C. Woody *et al.*, in *Proceedings of SCINT95*, Delft University Press, Delft, The Netherlands, (1996).
- [22] R.H. Mao, L.Y. Zhang and R.-Y. Zhu, *IEEE Trans. Nucl. Sci.* **57** (2010) 3841.
- [23] D.F. Anderson *et al.*, *IEEE Trans. Nucl. Sci.* **NS-40** (1993) 546-551.